ACS APPLIED NANO MATERIALS

www.acsanm.org Article

Electrofluidynamic Patterning of Tailorable Nanostructured Substrates for Surface-Enhanced Raman Scattering

Paulo De Carvalho Gomes, Jonathan James Stanley Rickard, and Pola Goldberg Oppenheimer*

Cite This: *ACS Appl. Nano Mater.* 2020, 3, 6774–6784 Read Online

ACCESS | Metrics & More | Article Recommendations | Supporting Information

ABSTRACT: The unique attributes of surface enhanced Raman spectroscopy (SERS) make it well suited to address the challenges associated with portable diagnostics. However, despite the remarkable progress in this field, where the instrumentation has made great strides forward providing a route to the miniaturization of sensing devices, to date producing three-dimensional low-cost SERS substrates which simultaneously fulfill the multitude of criteria of high sensitivity, reproducibility, tunability, multiplexity, and integratability for rapid sensing has not yet been accomplished. Successful implementation of SERS requires readily fine-tuned nanostructures, which create a high enhancement. Here, an advanced electrofluidynamic patterning (EFDP) technique enables rapid fabrication of SERS active topographic morphologies with high throughput and at a nanoresolution via the spatial and lateral modulation of the dielectric discontinuity due to the high electric field generated across the polymer nanofilm and air gap. The subsequent formation of displacement charges within the nanofilm by coupling to the electric field yield a destabilizing electrostatic pressure and amplification of EFDP instabilities enabling the controllable pattern formation. The top of each gold coated EFDP fabricated pillar generates controllable high SERS enhancement by coupling of surface plasmon modes on top of the pillar, with each nanostructure acting as an individual sensing unit. The absolute enhancement factor depends on the topology as well as the tunable dimensions of the nanostructured units, and these are optimized in the design and engineering of the dedicated EFDP apparatus for reproducible, low-cost fabrication of the three-dimensional nanoarchitectures on macrosurfaces, rendering them for easy integration in further lab-on-a-chip devices. This unique combination of nanomaterials and nanospectroscopic systems lay the platform for a variety of applications in chemical and biological sensing.

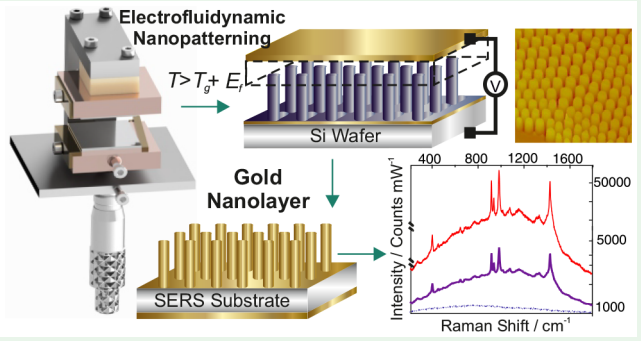

KEYWORDS: *electrofluidynamic patterning, SERS, tuneability, reproducibility, lithographically defined nanostructures substrates*

INTRODUCTION

Surface enhanced Raman spectroscopy (SERS) has been undergoing a renaissance in the past decade, on a trajectory to become the best-positioned analytical technique to posture significant impact on portable sensing. SERS, due to its distinctive attributes of rapid detection, high-sensitivity heightened with the capability of detection down to single molecule levels[1−7] as well as multiplexing, all while requiring no complex sample preparation, can be easily deployed for a breadth of applications ranging from homeland security through to medical diagnostics and biochemical sensors and onto food pathogenesis. Nevertheless, in spite of the large SERS related research activity being pursued, the field still poses many challenges to be addressed due to the numerous requirements with the majority of which have to be fulfilled simultaneously for it to become a widely established sensing tool. Although any imperfections in substrates have a significant effect on the definitive response, SERS-active platforms are often plagued by irreproducibility, instability, and a lack of tunability toward specific molecules. While high-enhancement is possible with SERS-active nanoparticles (NPs), only a miniscule fraction exhibits SERS activity, which also have a high-sample variability and poor batch-to-batch reproducibility, all substantially affecting the reproducibility of the measured signal.[8−12] This is exacerbated by both the use of surfactants to stabilize the NPs and the control of their shapes and aspect ratios, which in turn tend to reduce the subsequent attachment of the target analytes as well as the lack of established methods to further assemble the fabricated SERS-active NPs into distinctive "hot-spots" on macroscale ranges. Furthermore, SERS substrates with tunable localized surface plasmon resonances (LSPR) which can be easily interfaced externally (*e.g.*, in electrochemical devices) or

Received: May 1, 2020
Accepted: June 22, 2020
Published: June 22, 2020

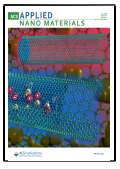

https://dx.doi.org/10.1021/acsanm.0c01190
ACS Appl. Nano Mater. 2020, 3, 6774–6784

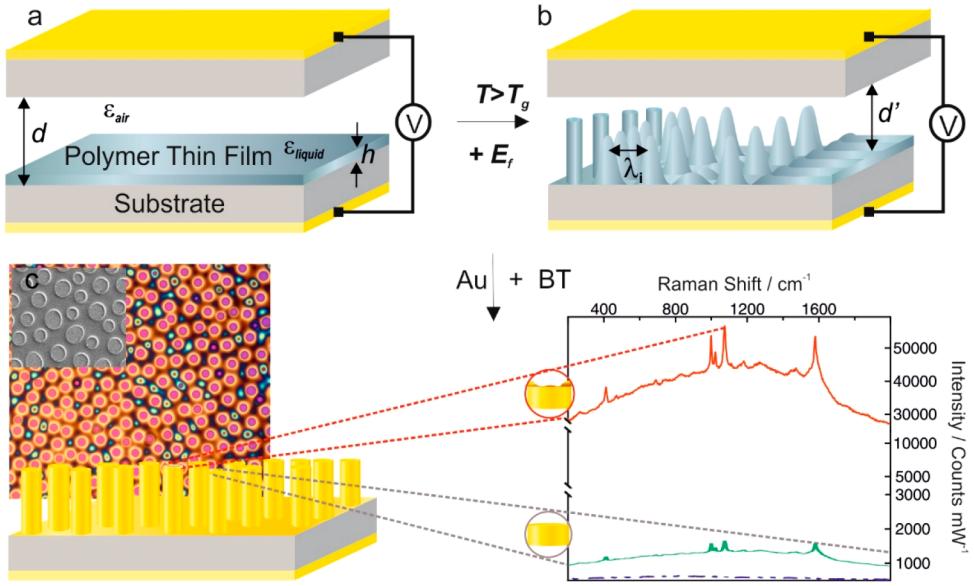

Figure 1. EFDP process for SERS fabrication. To commence the pattering process, (a) a thin polymer film with an initial film thickness h is deposited between two electrodes spaced apart by a distance d. Applying an external voltage, V and liquefying at $T > T_g$ leads to the generation of a high electric field, E_f ($\sim 10^8$V/m) within the microcapacitor and (b) formation of an instability throughout the film with a characteristic wavelength λ, which determines the pitch between the final structures. The increasing amplitude of the film variations guides the film's redistribution, which eventually spans the gap between the two electrodes. (c) Top-view optical microscopy and (inset) scanning electron microscopy images of the EFDP generated polymer structures, which are subsequently coated with a plasmon active gold nanolayer leading to high SERS signal enhancement. (inset) Representative SERS spectra of BT on top of various topologies of the formed pillars exemplifying that the roughened center surrounded by a nanorim (top view, red) yields more than 50 times higher signal enhancement relative to the flat pillar topology.

integrated internally (*e.g.*, inside microfluidic chips) are needed to gain the required consistent tailored high enhancement, a challenging task for NPs-based SERS systems. Therefore, lithographically structured substrates exhibit a great potential to intrinsically overcome these problems for enabling consistently reproducible SERS measurements. However, despite the significant advances of patterning methods and enhanced microfabrication techniques, the vast majority of synthetic "bottom-up" and "top-down" routes to generate SERS nanostructures are still based on conventional lithographic approaches. These include for instance photolithography, electron beam lithography, and focused ion beam (FIB), which are not only time-consuming and cumbersome but also require precise integration of multistep processes,[8,10,12−15] limiting the scalability of the resulting platforms, resulting in substrates that are far too expensive for practical applications. Inadequate resolution of the mold, two-dimensionality, the inevitable defects, poor mechanical stability, and pattern distortion collectively constitute the further limiting factors of micronanolithographies and other imprinting techniques. The fluctuating SERS enhancement measured across a single as well as seemingly identical substrates further exacerbate the downsides of the current fabrication processes. These limitations have driven extensive efforts to explore novel processes for the fabrication of highly ordered 3D structures with nanometer periodicities and underline the continuous, unmet need for high-throughput, reliable, and cost-effective methods to develop tunable, three-dimensional micronanoarchitectured surfaces to deliver highly reproducible, laterally and spatially consistent SERS enhancement.[16−18]

Here, we have developed an advanced technique of fabricating highly reproducible structures via the controllable electrofluidynamic patterning (EFDP) combined with a novel nanolithographic device to enable the needed level of control required to generate tailor-made, structured submicrometer SERS platforms (Figure 1) with fine-tuned nanoarchitectures (in contrast to the NPs) wherein uniquely, each of the individual structural units yields a high enhancement. Importantly, this is in contrast to the typically SERS active substrates, which act as collective surfaces for signal augmentation and which often encounter numerous difficulties in controlling the fabricated morphologies ranging from nano- to micrometer scale onto the overall macrosurface. We have previously demonstrated the use of the combination of the electric field and the hydrodynamics for lithography by patterning dielectric materials, conductive and crystalline materials, superapolar lotus-to-rose hierarchical nanosurfaces, with controllable alignment of the internal nanomorphologies.[19−23] Building upon these principles, in this study we systematically explore the localized plasmons in different nanogeometries, delivering an intuitive guidance for appropriate nanostructure design and introducing intelligent engineering of a novel nanolithographic device, which is further exploited to fabricate and control the metallic nanomorphologies with an inherent nanoroughness for tunable surface enhanced Raman spectroscopy. Optimized EFDP further enables the controllable fabrication of the desired platforms for multiplexed SERS detection. Building upon the vibrational spectroscopy principles, intimately dependent on the interplay between the laser excitation wavelength and the structural unit shapes and dimensions, we have further carried out an in-depth characterization and optimization of the EFDP generated architectures to enable the fabrication of tailor-made SERS substrates (Figure 2). Tuneability of the structural dimensions was possible via the independent control of various experimental parameters. For instance, the strength of the applied voltage (and thus, the generated electric field) allowed us to control the speed and the consistency of the patterning as

https://dx.doi.org/10.1021/acsanm.0c01190
ACS Appl. Nano Mater. 2020, 3, 6774−6784

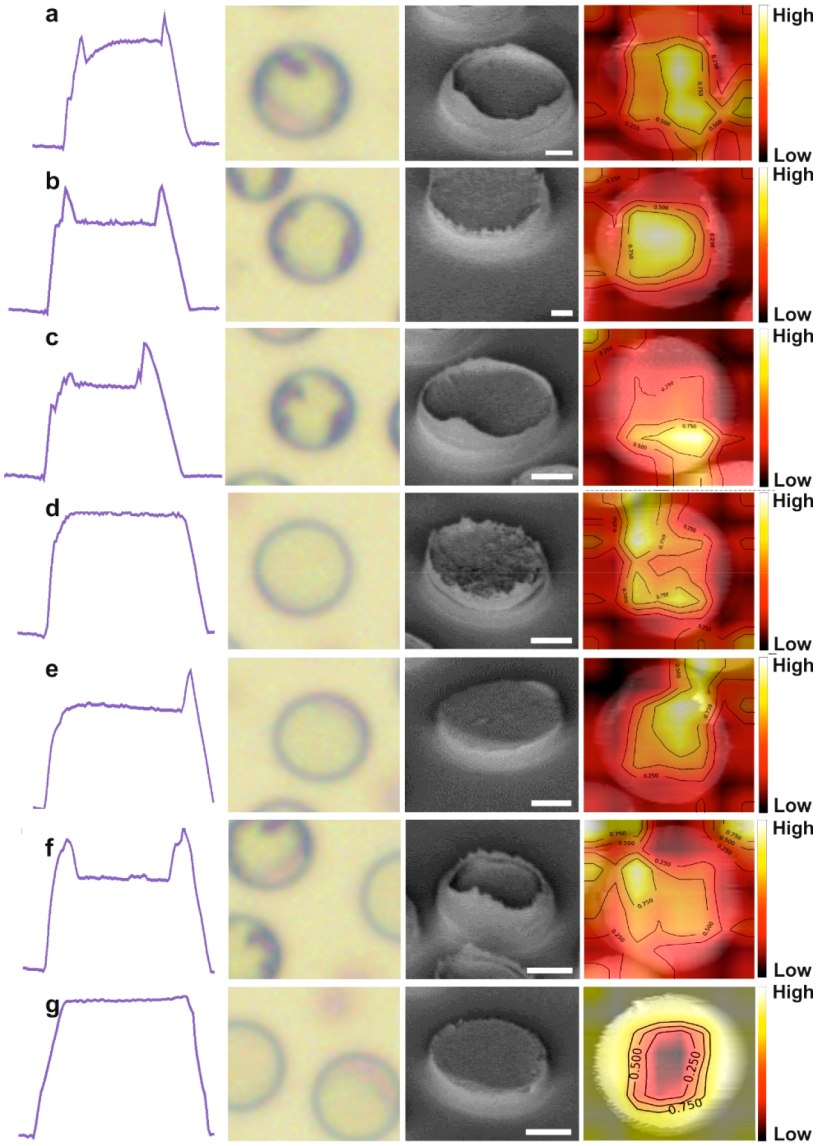

Figure 2. Representative EFDP-generated topological overview. Cross-section AFM profiles, top-view OM images, SEM micrographs, and DNN images of the EFDP generated structures. Corresponding SERS enhancements are shown in Figure 3d. (a) Pillar with H_{rim} = 250 nm and a nanoroughened center, EF = 9.0 × 10^6. (b) Pillar with an equivalent nanorim of H_{rim} = 300 nm and a roughened center, EF = 1.1 × 10^7. (c) Pillar with a one-sided nanorim of H_{rim} = 270 nm and a roughened center, EF = 8.8 × 10^6. (d) Pillar with nanoroughness throughout and no rim, EF = 6.4 × 10^6. (e) Smooth pillar with one-sided nanorim of H_{rim} = 200 nm, EF = 6.1 × 10^6. (f) Pillar with a nanorim of H_{rim} = 150 nm, EF = 6.7 × 10^6. (g) Smooth pillar top with no rim, EF = 5.8 × 10^6. Scale bar $_{SEM}$: 1 μm.

well as dictate the characteristic wavelength of the instability which, in turn, determined the spacing/pitch between the fabricated pillars. The filling ratio enabled the regulation of the structures' diameters. The small gap between the electrodes was carefully adjusted via the use of (nano) spacers with various dimensions which, in turn, controlled the achievable heights of the structures. Tuning of any of these parameters allowed the fabrication of controllable diameter, height, and pitch, all dictating the optical responses of the structures. This tunability yielded the subsequent design of substrates that generate strong localized electromagnetic fields at optical wavelengths that are required for the optimum SERS excitation by different laser sources. Interestingly, depending on the EFDP generated topographic morphologies of the top structural individual unit surfaces, which varied between a nanorim, planar, or roughened top, certain topologies exhibited considerably more enhanced SERS signal, which further guided the design of the dedicated electrode for reproducible fabrication of SERS substrates with optimum performance. Subsequently, a novel apparatus for fabricating high-precision, controllable EFDP SERS-active platforms with optimal structural parameters for reproducible SERS was designed and engineered. Validation bioassay comprised of the gold coated predesigned pillar structures are further utilized for rapid detection of traumatic brain injury indicative biomarkers, demonstrating that patterned EFDP arrays can act as straightforward and cost-effective substrates for high-throughput SERS detection. Overall, EFDP-based patterning postures salient advantages over other lithographic methods, including the inherent tunability of the fabricated nanoarchitectures (via directly adjusting the various experimental parameters), straightforward single-step patterning, the speed of which can be easily controlled via the chosen material to be patterned (with the instability being directly proportional to the

https://dx.doi.org/10.1021/acsanm.0c01190
ACS Appl. Nano Mater. 2020, 3, 6774−6784

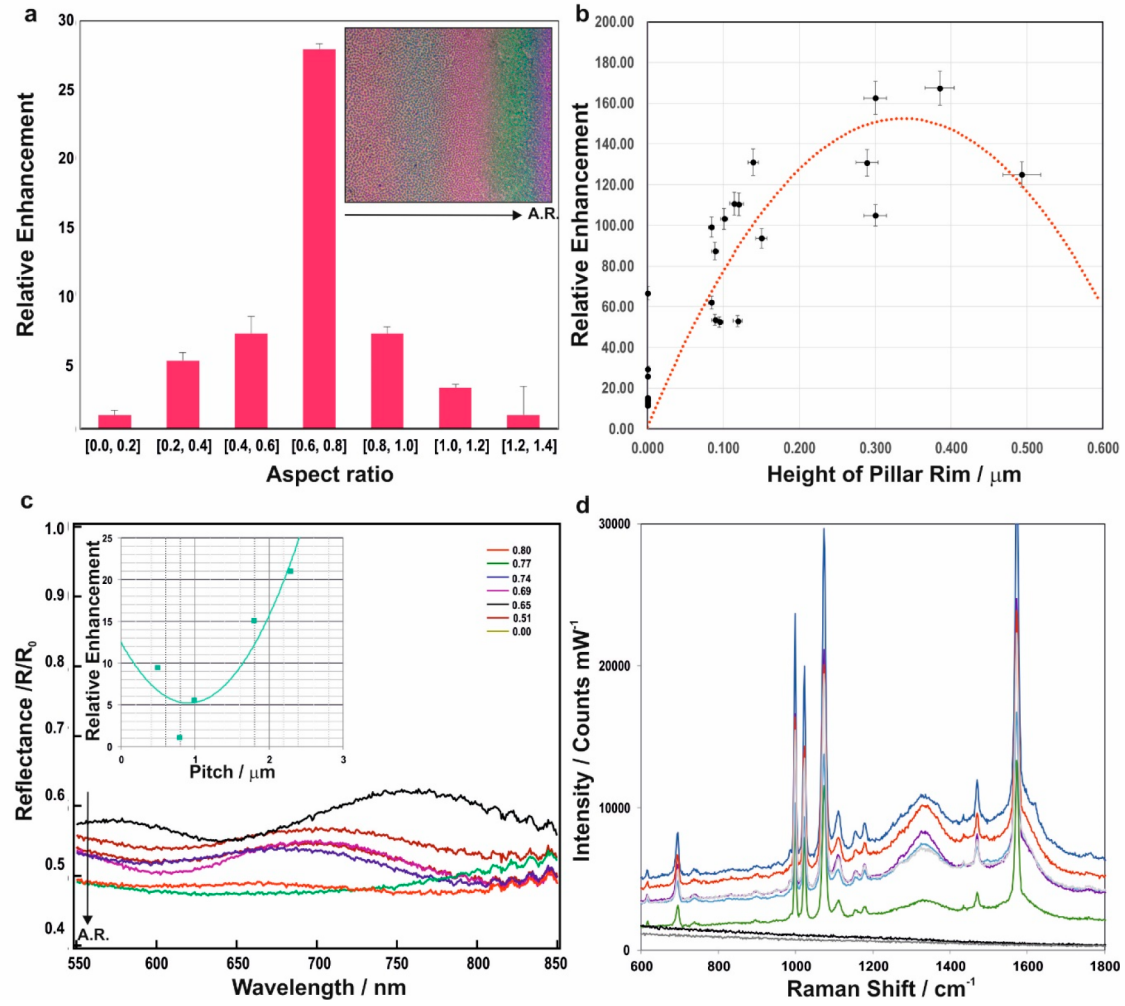

Figure 3. Tunability of structural dimensions of the metallo-dielectric EFDP fabricated SERS substrates for controllable and optimal plasmon excitations. (a) Relative SERS enhancement versus the AR identifies an optimal AR for signal enhancement in the range between 0.6 and 0.8. Wedge-geometry induced AR variation generates bands of color, due to the film thickness redistribution on top of the underlying silicon wafer, corresponding to the various aspect ratios (inset). The arrows correspond to the variation in AR and the corresponding color change across the sample. (b) Relative SERS enhancement of the benzenthiol's 1070 cm^{-1} peak with varying nanorim heights indicate an optimal range of H_{rim}~300 ± 37 nm. (c) Spectrally resolved reflectance spectra relative to the flat gold, R_0 as a function of the ARs. An increasing AR results in an increase in the extinction (R/R_0) due to the enhanced coupling of light into LPSRs, which are tuned by the pillar geometry. (inset) The variation of the enhancement as a function of the gap between the pillars at the excitation wavelength of 785 nm reveals another important parameter, tunability of which and its effect on strength of localized surface plasmon resonances and surface Raman enhancement allows the optimization of the fabricated substrates. (d) Characteristic Raman peaks of benzenethiol at 1000, 1070, and 1575 cm^{-1} readily detected in the spectra acquired from the EFDP SERS substrates showing the signal enhancement variation with the pillar's topological features shown in Figure 2.

viscosity[21,24]), cost-effectiveness of the fabricated substrates (made from low-cost polymers coated with a gold nanolayer), scalability, and the ease of integration within a lab-on-a-chip. These characteristics lay the basis for the design of highly reproducible SERS-active arrays with controllable localized plasmonic fields for a variety of lab-on-chip sensing devices.

RESULTS AND DISCUSSION

The EFDP method of fabricating a platform for SERS comprises assembling a microcapacitor device with bottom and top surfaces, facing each other, used as two opposing electrodes. A thin polymer film with an initial thickness, h (h = 80−100 ± 21 nm) is deposited on a bottom electrode, and a second top planar electrode is placed at a controllable distance, d (d = 150−800 ± 53 nm), leaving a certain air gap, which can be adjusted to micronanometer levels of precision (Figure 1a). The layered system is therefore equivalent to a sum of two capacitors in series filled-in with polymer and air layers. Subsequently, the film is fluidified, by heating the whole microcapacitor to an elevated temperature (i.e., above the glass transition temperature, T_g, of the polymer film) and in parallel applying an external voltage, V, which in turn generates a high electric field, E_f (~10^8 V/m) within the small capacitor's nanogap, d' across the dielectric material. The EFDP induces and successively exploits the evolving surface instabilities to generate tunable lithographically defined structural morphologies on the bottom electrode. For the sufficiently strong E_f generated inside the microcapacitor, the destabilizing electrostatic pressure, p_{el} overcomes the stabilizing effects of the Laplace pressure, p_L acting at the liquid−air interface (eq 1), which in order to minimize the free electrostatic energy of the system acts to align the interface, separating the two media, in parallel to the E_f lines:

https://dx.doi.org/10.1021/acsanm.0c01190
ACS Appl. Nano Mater. 2020, 3, 6774−6784

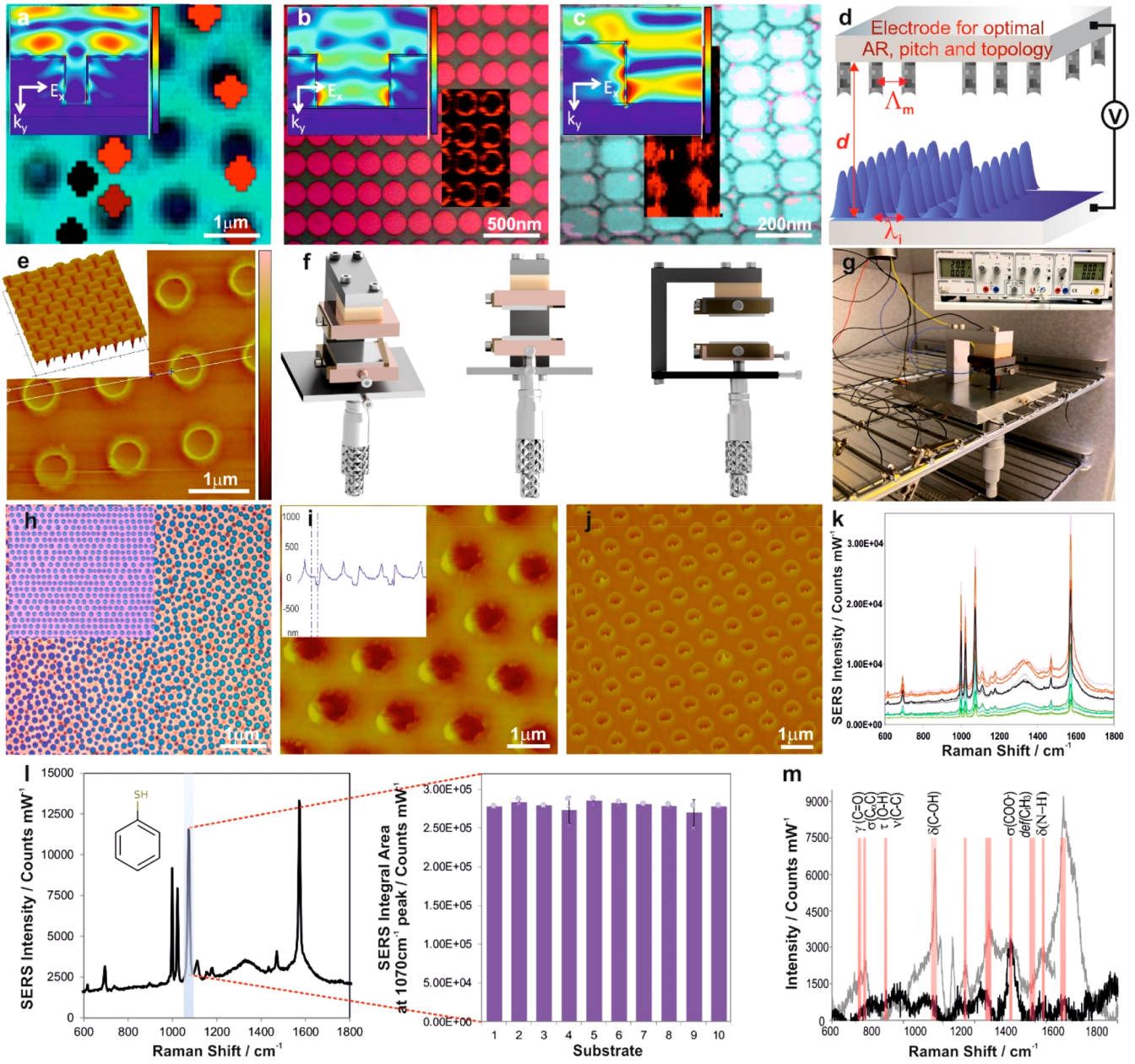

Figure 4. Engineering the EFDP apparatus and reproducibly controllable structures. (a–c) Optical microscopy images and the overlaid Raman maps with the corresponding 2D near-field simulations of the E_f distribution (insets) of the SERS enhancement occurring (a) exclusively on top of each pillar, (b) at the perimeter of the pillar, and (c) between the pillars. Schematics (d) and AFM 3D images of the fabricated (e) top electrode with carefully designed parameters including the interelectrode spacing, AR, pitch, and the interstructural spacing of the protrusions, Λ_m. (f) 3D schematic representation of the controllable EFDP rig. (g) Photograph of the EFDP prototype apparatus in the heating chamber. (h) OM image of pillars formed under the reproducible FEDP microlithography using planar top electrode, generating a homogeneous electric field throughout the capacitor, and (inset) pillars forming using lithographically predefined top electrode, introducing a heterogeneous electric field. AFM phase (i), with the corresponding 3D profile, and height (j) images of the high-fidelity EFDP-replicated patterns. (k) Reproducible substrates provide a highly consistent SERS signal over the entire substrate surface area. (l) Representative SERS spectrum of BT on a uniform substrate for the highlighted 1070 cm^{-1} peak, at an excitation of 785 nm laser, demonstrating reliable signal and substrate reproducibility (inset) of the SERS intensities on the EFDP generated arrays from 10 randomly selected positions on the gold-coated EFDP fabricated pillars. (m) Spike-and-recovery bioassay differentiates the characteristic peaks of biomarker in an artificial plasma with known concentrations (50 pg/mL). SERS spectra of the spiked (gray) versus normal, nonspiked (black); analyte was spiked into the test sample matrix, and its response was recovered in the assay by comparison to an identical spike in the standard diluent with 95.5 ± 3.4% recovery of the biomarker.

$$p_{el}\left(= -1/2\varepsilon_0\varepsilon_p(\varepsilon_p - 1)E_f^{\,2}\right) > p_L\left(= -\gamma\frac{\partial^2 h}{\partial x^2}\right) \quad (1)$$

where ε_0 is the dielectric permittivity of the vacuum, ε_p is the dielectric constant of the polymer, and γ is the surface tension. Consequently, the thin polymer film adopts a profile of pillars forming on the bottom substrate that correspond to the locations of the initially induced perturbations (Figure 1b).

Once the EFDP is complete, the electric field is maintained while the temperature is allowed to drop to below the fluidifying transition temperature, i.e., the T_g of the polymer,

https://dx.doi.org/10.1021/acsanm.0c01190
ACS Appl. Nano Mater. 2020, 3, 6774–6784

and the bottom substrate is released. This preserves the final structures intact and avoids fluctuations in the polymer or distortions. Subsequently, coating the EFDP generated submicron architectures with a plasmon-active gold nanolayer (25.0 ± 2.7 nm) yields effective enhancement of the local electromagnetic field (Figure 1c). EFDP thus enables a single-step fabrication of submicron SERS active substrates, with each of the individual pillars yielding a considerable signal enhancement (Figure 1c and Figure 3).[20−22,24]

The EFDP technique allows the patterning of micron and nanostructures with a broad range of feature sizes and topological morphologies of the final structural units (Figure 1c, inset and Figure 2). These can be accomplished by either alternating the termination time of the patterning process, which can lead to either conelike structures or sharp pyramids with a round base or alternatively, due to the disassembly process of the top electrode can lead to the variation in shape and roughness of the tops of the formed structures. Salinizing the top electrode prior to the onset of the patterning process renders it apolar to surfaces grafting a monolayer of octadecyltrichlorosilane between the upper and lower substrates and facilitates the smooth release of the substrates. This enables easy disassembly due to the nonsickly self-assembled nanolayer. Alternatively, it is possible to directly disassemble the microcapacitor setup without any additional salinization steps. These enable the production of a range of structures where the top surface of each pillar is either smooth, concave, roughened, or a combination of those (Figure 2). Out of these, certain structural topologies were found to provide a further degree of signal enhancement on top of each pillar (Figure 1c, inset). Representative EFDP micronanoarchitectures' cross-section atomic force microscopy (AFM) profiles, bright field optical microscopy (OM) top-view images, scanning electron microscopy (SEM) images, and deep neural network (DNN) images are shown in Figure 2. The DNN algorithm for image classification of the EFDP patterned structures for SERS labeling includes several stages (see Methods for details): (i) data gathering, (ii) data preprocessing, (iii) data augmentation, (iv) feature extraction using a pretrained convoluted neural network, followed by (v) fine-tuning and the visualization of the activated neurons for the image classification. DNN images allow the classification of the formed pillars as a function of the enhancement and, thus, the correlation of the images with the degree of enhancement of the scattered radiation. The results from our data show that the center of the smooth pillar tops has exhibited weak activation regions for "SERS"-like features while the nanorim like edges exhibited highly activated regions indicating those being an important factor for "SERS" active DNN neurons. The various generated geometries and topologies of the pillars included the flattop with no rim, equivalent nanorim surrounding roughened or smooth centers, with various rim heights, H_{rim} ($0 \leq H_{rim} \leq 500$ nm) and one-sided nanorim. A standard analyte of benzenethiol (BT) was subsequently used to evaluate the SERS enhancement factor (EF) from each of these different patterns, acquired under identical experimental conditions (Figure 3d and Figures S1 and S2). Establishing optimal top feature morphologies is used in the subsequent design of the dedicated top electrode in conjunction with the controllable microlithographic EFDP apparatus.

Subsequent to identifying optimal candidate topologies for achieving increased EFs, we have investigated the impact of other structural parameters, all of which can be tuned during the EFDP process, on the resulting signal enhancement. A systematic analysis reveals that the relative signal enhancement strongly depends on the aspect ratio (AR) of the pillars, highlighting a key factor for the design of optimized EFDP-generated SERS-active substrates (Figure 3a). Furthermore, due to the slight misalignment of the capacitor plates in the EFDP capacitor, there is a "wedge" geometry across the substrate with a variation ranging from 100 nm to 1 μm across for a 1 cm wide sample, which subsequently leads to the lateral variation in the resultant pillar's aspect ratio. This has been exploited to our advantage to generate a breadth of pillars with varying height and diameters. In the fabricated surfaces it was found that, the ratio of the thickness of one film coating on the surface of the substrate to the diameter of the formed structure should be at least 0.6 and no more than 0.8 for the optimal SERS enhancement factor (Figure 3a). The height of the rim-like topology in the formed pillar was found to have an optimal range with $0.30 \leq H_{rim} \leq 0.37$ μm exhibiting the highest achievable signal enhancement (Figure 3b).

The generated pillars of the bottom substrate, once adopted, are spaced from one another at a certain pitch distance, λ. During the EFDP, the step of adjusting the gap between the top and bottom electrodes to a micrometer level of precision and further adjusting the gap to a nanometer level of precision can be used to control the spacing between adjacent pillars. This pitch, λ, can additionally be controlled by alternating the strength of the applied electric field. The influence of the pitch on the resulting SERS signal shown in the inset of Figure 3c demonstrates that the electric field excited on the gold coated structures has a local minimum at $\lambda = 1$ μm and otherwise increases considerably at $\lambda > 1$ μm. Furthermore, depending on the pillar's interstructural pitch, patterned arrays can exhibit SERS enhancement either on top of each individual structure (Figure 4a), at their perimeter (Figure 4b) or in the area between the structures (Figure 4c). The spacing of the pillars is thus also of an importance to the localization of the enhancement and the "correct" pitch ($1.2 \leq \lambda \leq 2.5$ μm) can assist in enabling each pillar to act as an individual detection center.

Dependence of reflectance with the wavelength reveals increasing intensity with an increasing aspect ratio up to optimal dimensions at AR = 0.80 ± 0.12, variation that mainly arises from coupling of light into plasmon resonances, which are tuned by the pillar dimension, and therefore, the relative SERS enhancement is correlated with the increased strength of plasmonic coupling into the structure. Experimentally measured reflectance across pillars, R/R_0 with laterally varying ARs exhibits increased extinction with an increasing aspect ratio, with a nearly 30 percent increase that occurs in extinction when the AR varies from 0.5 to 0.8 (Figure 3c).

Evaluation of the SERS signal evolving from each of the representative topological morphologies in Figure 2 demonstrates variation in the enhancement factor of up to 40% between the highest and the lowest enhancing pillars. The absolute EF for the optimal pillar with an equivalent nanorim of H_{rim} = 300 nm and roughened center was found to be $1.1 \times 10^7 \pm 1.7 \times 10^6$ in contrast to the smallest enhancement achieved from the smooth pillar with no rim with an EF of $5.8 \times 10^6 \pm 1.2 \times 10^6$ using a 785 nm excitation laser. It is plausible that the EFDP structures with optimal enhancing AR and nanorim like topology with a nanorough center create a coupling effect combining the plasmon and whispering-gallery resonance for trapping and enhancing the signal. Such optical

https://dx.doi.org/10.1021/acsanm.0c01190
ACS Appl. Nano Mater. 2020, 3, 6774−6784

"nanocavities" could be confining light to smaller volumes by resonant photon circulation and thus yielding an improved SERS enhancement. For the subsequent reproducible pattern design, a pillar with an equivalent nanorim and roughened center was found to be a favorable topology with the optimal feature sizes of these pillars identified to preferably have an AR ~0.7−0.8, rim height of 300 nm, and $1.2 \leq \lambda \leq 2.5$ μm.

Establishment of the EFDP structural factors for optimal SERS enhancement has subsequently guided the fabrication of reproducible and controllable three-dimensional SERS substrates via designing and engineering a novel high-precision lithographic rig in conjunction with the dedicated top electrode. The developed microlithographic setup combines micromanipulator and piezoactuators for the finest adjustments to enable parallel capacitor-like EFDP patterning for consistent fabrication of submicron pillars (Figure 4f). It is designed to allow for several degrees of freedom of movement and well-aligned parallel positioning of the top and bottom electrodes, to yield the integrity and accuracy of the intercapacitor distance down to the submicron scale, for the fabrication of highly reproducible SERS-active substrates with the ideal structural topological morphologies, aspect ratios, and pitches. The controllable microlithographic EFDP apparatus comprises a support for a bottom substrate that has a film coating on the top surface thereof and a second one facing the bottom and supporting a second top substrate with a controllable gap between the surfaces. The base of it is made of aluminum. Extending upward from the base is a pillar comprised of a rectangular aluminum pillar screwed to the base. Attached through an opening in the base is a micrometer, which has a nonrotating head, with a copper block mounted on its spindle. A bottom substrate to be patterned is mounted on the copper block. A spring clamp (a thin beryllium copper spring clamp) is used to hold the bottom substrate in place on the copper block, also ensuring electrical connection of the bottom substrate to ground. A spar that extends from the pillar, supports a top substrate assembly suspended over the bottom substrate. At the end of the spar a block of insulating PEEK is attached and then attached to that is a copper block with a spring clamp to which the top electrode/substrate is placed. The assembly includes a support arm underneath which is mounted a piezo-actuator, an upper block, a second piezo-actuator, a lower block, and the top substrate. The top substrate is clamped to the assembly using a beryllium copper spring clamp. The beryllium copper spring clamps are thinner than the height of the silicon substrates and hold the substrates at their edges to allow a bias voltage to be applied to the top and bottom substrates. A first gap adjustment enables adjustment to a micron scale precision, via a micrometer, with the second gap adjustment provided to allow adjusting the gap to the nanometer level (via piezo actuators) of precision, yielding a significant improvement in the reproducibility and thus the enhancement factor from the surface. The gap during the patterning is monitored by measuring the current flowing between the two electrodes using a micro-ammeter. Subsequently, a connection is provided to a source of electrical power for applying an electric field across the gap between the facing surfaces of the first and second substrates (Figure 4g). A sensor is concurrently used to sense a *finite* current flowing through the first and second substrates, and the whole apparatus is homogeneously heated to an elevated temperature to enable the thin film's fluidity. This further ensures that there is no temperature gradient around the substrates as well as allowing for more accurate control of the gap between the substrates.

While the surface of the upper electrode for the study and optimization of the EFDP structural parameters for SERS was a flat (planar) surface, in the reproducible microlithographic setup, the surface of the top electrode comprises a dedicated, carefully designed templated pattern of structures that protrude toward the surface of the bottom substrate. We have established that the highest EF of gold covered SERS active pillars is achieved when the color of the pillars is blue or green, corresponding to a pillar aspect ratio of 0.7−0.8, as shown in Figure 2a, inset. The design and fabrication of the dedicated top electrode's structures was thus dictated by the established optimal parameters of the EFDP yielding the formation of high fidelity positive replicas of the imposed morphology and fabrication of the structures in a more controllable and repeatable manner (Figure 4d,e). The master electrode is of a high structural integrity and durability and can be used to consistently produce structures of interest from low-cost materials using the EFDP to guide the pattern formation and, therefore, enabling high-reproducibility, cost-efficiency, and scalability of the generated nanosurfaces, rendering this technique even more technologically appealing. The uniquely designed top electrode does not only comprise the ultimate dimensions for high enhancement but also enables the creation of rimmed nanocavities and is comprised of downward protruding pillars with AR of 0.8, pitch of 1.2 μm, and H_{rim} = 300 nm nanorim on their perimeter (Figure 4d). Assembling this top electrode within the microlithographic EFDP apparatus (Figure 4g) and applying a voltage across the two plates yields the generation of a heterogeneous electric field. In this case, the liquefied polymer film is drawn toward the protrusions of the top electrode, where the electrostatic pressure is the highest and the destabilization process is the fastest, faithfully reproducing the imposed patterns as shown in Figure 4h−j. Guiding the uniform structures fabrication, the setup ensures that the protrusions match each other and the height of a given pillar substantially matches the height of another pillar. The AFM images show the reproducibly fabricated morphologies comprised of pillars with the optimized dimensions and topology spanning SERS substrate areas of 200 × 200 μm^2 with high fidelity patterns. Upon examining 10 arbitrary capacities across each substrate with the monolayer of BT as the SERS probe, the EFDP fabricated SERS surfaces exhibited reliable signal intensities and substrate reproducibilities. A repeatable SERS response was obtained from the pillars with average standard deviation of less than 3.0% in the framework of one sample (Figure 4I, inset and Figure S3) and between the different samples (height of the bars in Figure 4I, inset and Figure S3) for the 1070 cm^{-1} Raman peak comparable to the state-of-the-art SERS substrates.[25,26] Uniform SERS signal was also obtained across several substrates with the EF values being narrowly distributed around the average of $1.1 \times 10^7 \pm 4.3 \times 10^5$ (Figure S2b). For the 0.95 confidence interval data it is therefore, expected that the difference in EF as measured between the different areas to lie between (9.4×10^6, 1.1×10^7) for 95% of the future measurements. The experimentally calculated reproducibility coefficient indicates that the absolute difference between any three subsequent EF obtained on a particular substrate are estimated to be no greater than 8.55% on 95% of occasions. The wavelengths of the LSPR and the strength of the electric field are highly sensitive to the

https://dx.doi.org/10.1021/acsanm.0c01190
ACS Appl. Nano Mater. 2020, 3, 6774−6784

dimensions (*e.g.*, AR, diameter, pitch), the shape (the inherent nanoroughness in the central parts of the structures enclosed by the surrounding nanorim), and coupling modes of the nanostructures. The controlled pitch combined with the consistent nanorim topology (Figure 2 and Figure S1) renders the adjacent pillars not plasmonically coupled to each other, generating a strong localization on top of the structures (with the optical enhancement on the surface mainly due to red-shifted apex plasmons) and consequently, high fields and SERS enhancements, which arise almost exclusively from a single structure. The EF and sensitivity achieved with these nanomorphologies is of a similar magnitude to both the commercially available as well as the various SERS substrates demonstrated in the literature while exhibiting an improved signal reproducibility and stability.[16,17,27−40] EFDP-SERS substrates retain their structural integrity over the period of several months with no agglomeration or pattern distortion discovered. The substrates show excellent stability throughout the spectral collection period of 3 months with an average relative standard deviation of 3.9% (Figure S4).

To demonstrate the diagnostic potential of the developed EFDP SERS active substrates, we have assembled a proof-of-concept spike-and-recovery assay comprised of *N*-acetylaspartate spiked artificial blood plasma deposited on the fabricated substrates at a concentration of 50 picograms per milliliter. *N*-Acetylaspartate is a biomarker indicative of acute, early stage traumatic brain injury and is exclusively localized in neurons, reflecting their functional status (as well as of axons) in the brain.[41−43] It is considered a marker for neuronal health and viability, highly specific to the central nervous system, not released by other organs and thus, is a very sensitive measure of neuronal compromise. This biomarker is thus of importance for development of early stage triaging point-of-care diagnostic technologies for traumatic brain injuries. The EFDP-SERS substrates were used to establish the specific fingerprint spectra (Figure 4m and Figures S5 and S6) and to quantitatively determine the lowest detectable concentration of the target biomarker. The characteristic peaks of the analytes were monitored and a linear trend was observed with a good correlation (R^2 = 0.9910) between biomarker concentrations (100 nM to 1 pM) and SERS intensity (Figure S8). No signal enhancement was observed on the flat parts on the substrate between the pillars (Figure 4a, inset and Figure S7). SERS spectra for detection of the *N*-acetylaspartate show successful differentiation of the biomarker's fingerprints,[4244] spiked at known concentrations (Figure 4m) in the artificial plasma (top) versus the control sample (bottom), indicating the potential for detection and differentiation from clinical blood and plasma samples for future development of biodiagnostic SERS assays.

CONCLUSIONS

We have demonstrated a tailored approach for the manufacture of surface enhanced Raman scattering active nanoarchitectures via the EFDP lithography. The plasmon dependent phenomena of the fabricated substrates can be straightforwardly adjusted via the lithographic key-factors, allowing the development of reliably engineered and cost-effective substrates with reproducible and high SERS enhancement. SERS signal enhancement of these substrates is governed by not only the pillar's nanotopology but also by the dimensions of the fabricated structures, parametrized by the ratio of the height to diameter as well as the interstructural pitch. The controllable aspect ratio via the EFDP and its effect on strength of the enhancement factor thus further enables the possibility of fine-tuning the substrates responses for different laser excitation wavelengths. The ability to carefully design and fabricate highly reproducible optimized SERS active nanoarrays enables the control of localized plasmonic fields, laying a platform for developing portable lab-on-chip devices and sensors to detect and analyze a variety of biochemicals (Figure S9) pertinent for medical, environmental, and forensic applications. Intriguingly, due to the individually enhancing optimized structural units, each topological structure in the array could further be functionalized with specific receptors for a range target molecules for rapid, multiplexed, highly specific and sensitive detection. These will be, in turn, useful for the development of rapid-response, addressable miniaturized sensors, which are selective for targeted chemical and biological molecules.

METHODS

Materials. Polystyrene (PS, M_w 100 kg/mol, M_w/M_n < 1.07) was used as a polymer for the patterning (purchased from Polymer Standards Service GmbH) and toluene was used as a main solvent in this process (Fisher Scientific). Highly polished *p*-doped silicon (Si) wafers with ⟨100⟩ crystal orientation (Wafernet, GMBH, Eching, Germany) were used during the EFDP as bottom electrodes (*X-lith eXtreme* Lithography). 3 wt/wt % PS solutions were filtered through a Teflon filter with a pore diameter of 100 nm. BT (Analytical Standard, Sigma-Aldrich) was used without further purification. Silver paint (Electrodag 1415M) used to contact the electrodes. Standard biomarkers (S one-hundred calcium-binding protein B and *N*-acetyl aspartate) for individual fingerprint signature studies were acquired from the Human ELISA Kit (Abnova) and Sigma-Aldrich (Saint Louis, MO). The 99.999% purity gold target for sputtering was purchased from Kurt J. Lesker.

EFDP SERS Substrates Fabrication. PS was used as the polymer for thin film deposition and patterning during the EFDP, and highly polished p-doped silicon wafers were used as bottom and top electrodes in the capacitor setup. Silicon wafers were thoroughly cleaned in a "piranha" solution consisting of sulfuric acid and hydrogen peroxide (3:1, accordingly) followed by rinsing with deionized water and drying under nitrogen flow. An initial solution of PS in toluene 3% w/w was subsequently spin-coated onto the freshly cleaned 1.0 × 1.0 cm^2 silicon electrodes and these were then electrically connected to the external voltage supply and homogeneously heated to 175 °C. The whole EFDP patterning rig was enclosed inside a high-precision performance convection oven ensuring optimal temperature uniformity throughout the chamber. The temperature in the oven was thermostatically controlled (a thermometer was placed in an oven which was set at the desired operating temperature. The temperature reading of the thermometer was compared to the oven thermostat reading). Furthermore, a sensor was concurrently used to sense a *finite* current flowing through the first and second substrates and the whole apparatus was homogeneously heated to an elevated temperature to enable the thin film's fluidity. This has ensured that there was no temperature gradient around the substrates. Once the EFDP process has been completed, the capacitor setup was cooled down to room temperature to quench the formed structures and the external voltage supply was disconnected. To facilitate the smooth release of the patterned surfaces, the substrate was grafted with an octadecyltrichlorosilane self-assembled monolayer. The patterned substrates were finally coated with a gold nanolayer with an average thickness of 25.0 ± 2.7 nm (Emitech sputter-coater) using a DC argon plasma and a gold target. The gold deposition was performed onto all of the EFDP-generated substrates as well as the polymer film as reference. Subsequently, benzenethiol monolayer was assembled on the gold-coated surfaces from ethanolic solution at varying concentrations.

Fabrication of Top Electrode. Focused ion beam (FIB) process was used to fabricate the dedicated EFDP electrode. For this purpose,

https://dx.doi.org/10.1021/acsanm.0c01190
ACS Appl. Nano Mater. 2020, 3, 6774−6784

initially silicon wafers were cleaved and then cleaned using a carbon dioxide spray system. Subsequently, the electrode was produced using an FEI Helios Nanolab 650 dual beam scanning microscope, equipped with an electron beam for imaging and a separate beam of gallium ions at 52° to the electron beam. The gallium ions are accelerated up to 30 kV to provide them with a high energy and the generated beam of ions is focused to a spot by several electrostatic lenses and then scanned over the object by scan plates. The gallium ion beam was used to sputter away material to create the required patterns. The associated patterning system of the Helious (Nanobuilder) was further employed by using a bitmap image to control the ion beam to recreate the pattern from the designed image. Nanobuilder was subsequently used to shift the stage and repeat the process to create large patterned areas.

Raman Spectroscopy Measurements. SERS measurements were carried out using InVia Qontor spectrometer confocal Raman (Renishaw) equipped with 785 nm excitation laser, which was adjusted for optimal throughput, fluorescence control, and sensitivity. The spectra were typically acquired at 10 s exposure time and a laser power of 1−10 mW with a 785 nm laser to avoid photochemical effects in the SERS spectra, sample damage, or degradation. The equation of the linear fit obtained from the dilution studies quantitatively calculating the limit of detection as 3 times the standard deviation of the blank, derived from the gradient of the straight line, where σ is the standard deviation of the response and S is the slope of the calibration curve. SERS maps were generated in a Stream-line mode scan with an exposure time of 10 s and power of 5 mW at 785 nm. A 50× objective with a numerical aperture of 0.75 was used for SERS measurements over a range of 500 to 2500 cm^{-1} relative to the excitation Raman shift. Optical measurements were carried out with a specially adapted research grade microscope (Leica DM 2700M) equipped with an incoherent white light source, allowing confocal measurements with 2.0 μm depth resolution. The spectra were normalized with respect to those recorded on flat gold or gold-covered flat polymer film surfaces. An intelligent-fitting filter was applied for baseline subtraction.

Calculation of the SERS EF. Numerical modeling was carried out using a finite element solver COMSOL v4.3. The enhancement factor calculation is reproduced from ref 42. In brief, SERS enhancement factor was calculated by comparing the intensities of the unenhanced Raman scattering peak (I_{Raman}) at 1 070 cm^{-1} of pure BT obtained by focusing the laser into a quartz cell and the corresponding SERS signals (I_{SERS}) obtained from the SERS substrates. The detection volume of the solution-phase benzenethiol sample, V_f, was calculated using the following relation: V_f = (depth of focus) × (focus area) = $(1.4n\lambda/NA^2) \times \pi(0.4\lambda/2NA)^2$. The surface density of the adsorbed BT molecules on the structured surface was taken as ρ_s = 3.3 molecules/nm^2, and the enhanced area, A, was defined as the diffraction limited spot size ($\pi(0.4\lambda/2NA)^2$), with NA, numerical aperture; n, refractive index; λ, wavelength; ρ_v, surface density of molecules in the detection volume. The EF was calculated using the relation: $EF = [I_{SERS}/(\rho_s A)]/[I_{Raman}/(\rho_v V_f)]$.

Atomic Force Microscopy. A JPK NanoWizard II atomic force microscope was used to thoroughly characterize the surfaces' topography. The AFM measurements were performed using tapping mode via an intermittent contact of the tip with the sample in ambient conditions. NCHV-A cantilevers with a resonance frequency of 320 kHz and stiffness of 42 N m^{-1} were used. Height and phase images were analyzed with Gwyddion's software (version 2.55). The AFM measurements were used to acquire important parameters including the film thickness h, the interelectrode spacing d, the characteristic pitch λ, and the AR of the generated structures. A total of 13 areas of 50 × 50 μm^2 were scanned throughout each sample. The area was chosen according to the different colored regions of the EFDP samples. The heights ranging from 200 to 700 nm spanned a lateral distance of approximately 700 μm. Each scan was performed at 1024 × 1024 pixel quality at approximately 3 s/line raster rate, for a total of 1 h/region. The set point was adjusted for each region to compensate for the pillar height changes while the rest of the structural parameters were kept constant. Ten pillars were chosen per scanning region, totalling in 130 pillars characterized. The pillars were chosen as representative examples of the different topologies obtained during the EFDP lithography.

Optical Microscopy. For the concurrent tracking of the AFM images, a corresponding optical microscopic image of the pillars was also acquired. These optical images guided the navigation of the AFM measurements between different regions (Leica DM2700 M). Pattern formation in thin polymer films was qualitatively analyzed using bright-field reflection microscopy (Olympus Optical Microscopes GX61, GX2, and BX40). The reflection of white light from the sample enabled resolving the submicron-scale features. The evolving patterns were also observed by *in situ* monitoring of the EFDP pattern formation and replication in thin films using a digital camera and imaging software (Carl-Zeiss VisioCam, AxioVision).

Scanning Electron Microscopy. Samples for SEM imaging were prepared by placing a postexperiment, disassembled substrate with the generated patterns on an inclined or cross-sectional holder to enable the imaging of the top and cross-sectional views. Scanning electron micrographs were acquired using a thermally assisted field emission source scanning electron microscope (FEI helios dual beam) with a lateral resolution of 2−5 nm with a typical acceleration voltage of 1−10 kV.

Deep Neural Network Image Analysis. For the data gathering stage, the studied individual pillars were in the range of heights varying between 200 and 700 nm and diameters of 0.5−5 μm. All the images were acquired as a top view and height differences are given by a different intensity level on the grayscale. The ability of the pillar to enhance the signal was either labeled as "No enhancement", meaning there is no or negligible Raman signal enhancement on the pillar and as "SERS" where there is a noticeable signal enhancement from the pillar. Each of the chosen pillars was then characterized via the AFM and the corresponding surface profiles were also obtained. These constitute the initial data set for the DNN. The subsequent step of the data preprocessing included ensuring that all the images are on the identical grayscale and same pixel size. For the data augmentation, the data set was increased by conducting rotations and inversions of the acquired images while keeping the labels fixed. This is possible due to the fact that the Raman measurements are the same for the pillar independent of the rotation. Following the data augmentation, a complete training data set is generated. In the next step, a VGG16 pretrained convnet was used, which was later modified with a fully connected classifier by changing the output layer to "SERS" and "No enhancement" and subsequently, the last block of neuron layers prior to the classification was fine-tuned. After training the modified model with the data set, it was tested with the data set, where the testing data included pillar images that were never "seen" by the model. This information identifies the features that are most important for the SERS-active pillar via the class activation map (CAM) by producing a heat map image of the neuron activation over the input test image for a specific label, which results in how intensely the input image activates a given label. The overlaid heat map has consequently a high activity on features of the input image that are "SERS"-like features.

■ ASSOCIATED CONTENT

Supporting Information

The Supporting Information is available free of charge at https://pubs.acs.org/doi/10.1021/acsanm.0c01190.

Characterization of the reproducibility of the EFDP substrates and EFs, stability analysis, characteristic fingerprint SERS spectra with a barcode of peaks of the studied biomarkers, and quantitative detection analysis via EFDP-SERS (PDF)

■ AUTHOR INFORMATION

Corresponding Author

Pola Goldberg Oppenheimer − *School of Chemical Engineering, Advanced Nanomaterials Structures and*

https://dx.doi.org/10.1021/acsanm.0c01190
ACS Appl. Nano Mater. 2020, 3, 6774−6784

Applications Laboratories, College of Engineering and Physical Sciences, University of Birmingham, Birmingham B15 2TT, U.K.; Healthcare Technologies Institute, Institute of Translational Medicine, Birmingham B15 2TH, U.K.; orcid.org/0000-0002-1014-4724; Email: GoldberP@bham.ac.uk

Authors

Paulo De Carvalho Gomes − *School of Chemical Engineering, Advanced Nanomaterials Structures and Applications Laboratories, College of Engineering and Physical Sciences, University of Birmingham, Birmingham B15 2TT, U.K.;* orcid.org/0000-0003-2986-1157

Jonathan James Stanley Rickard − *Department of Physics, Cavendish Laboratory, University of Cambridge, Cambridge CB3 0HE, U.K.;* orcid.org/0000-0002-5423-9979

Complete contact information is available at: https://pubs.acs.org/10.1021/acsanm.0c01190

Notes

The authors declare no competing financial interest.

■ ACKNOWLEDGMENTS

We acknowledge funding from the Wellcome Trust (Grant 174ISSFPP), the Royal Academy of Engineering (Grant RF1415\14\28), and the EPSRC. P.G.O. is a Royal Academy of Engineering Research (RAEng) Fellowship holder.

■ REFERENCES

(1) Han, X. X.; Ozaki, Y.; Zhao, B. Label-Free Detection in Biological Applications of Surface-Enhanced Raman Scattering. *TrAC, Trends Anal. Chem.* **2012**, *38*, 67−78.

(2) Han, X. X.; Zhao, B.; Ozaki, Y. Surface-enhanced Raman Scattering for Protein Detection. *Anal. Bioanal. Chem.* **2009**, *394* (7), 1719−1727.

(3) Kahraman, M.; Mullen, E. R.; Korkmaz, A.; Wachsmann-Hogiu, S. Fundamentals and Applications of SERS-based Bioanalytical Sensing. *Nanophotonics* **2017**, *6*, 831−852.

(4) McQueenie, R.; Stevenson, R.; Benson, R.; MacRitchie, N.; McInnes, I.; Maffia, P.; Faulds, K.; Graham, D.; Brewer, J.; Garside, P. Detection of Inflammation in Vivo by Surface-Enhanced Raman Scattering Provides Higher Sensitivity Than Conventional Fluorescence Imaging. *Anal. Chem.* **2012**, *84* (14), 5968−5975.

(5) Moore, T.; Moody, A.; Payne, T.; Sarabia, G.; Daniel, A.; Sharma, B. In Vitro and In Vivo SERS Biosensing for Disease Diagnosis. *Biosensors* **2018**, *8* (2), 46−71.

(6) Wang, R.; Chon, H.; Lee, S.; Ko, J.; Hwang, J.; Choi, N.; Cheng, Z.; Wang, X.; Choo, J. Biomedical Applications of Surface-Enhanced Raman Scattering Spectroscopy. In *Frontiers and Advances in Molecular Spectroscopy*; Laane, J., Ed.; Elsevier, 2018; Chapter 9, pp 307−326.

(7) Wang, Y.; Kang, S.; Khan, A.; Ruttner, G.; Leigh, S. Y.; Murray, M.; Abeytunge, S.; Peterson, G.; Rajadhyaksha, M.; Dintzis, S.; Javid, S.; Liu, J. T. C. Quantitative Molecular Phenotyping with Topically Applied SERS Nanoparticles for Intraoperative Guidance of Breast Cancer Lumpectomy. *Sci. Rep.* **2016**, *6*, 21242−21254.

(8) Ackermann, L.; Althammer, A.; Born, R. Catalytic Arylation Reactions by C−H Bond Activation with Aryl Tosylates. *Angew. Chem., Int. Ed.* **2006**, *45* (16), 2619−2622.

(9) Kho, K. W.; Qing, K. Z. M.; Shen, Z. X.; Ahmad, I. B.; Lim, S. S. C.; Mhaisalkar, S.; White, T. J.; Watt, F.; Soo, K. C.; Olivo, M. Polymer-Based Microfluidics with Surface-Enhanced Raman-Spectroscopy-Active Periodic Metal Nanostructures for Biofluid Analysis. *J. Biomed. Opt.* **2008**, *13* (5), 054026.

(10) Lim, C.; Hong, J.; Chung, B. G.; deMello, A. J.; Choo, J. Optofluidic Platforms Based on Surface-enhanced Raman Scattering. *Analyst* **2010**, *135* (5), 837−844.

(11) Pennathur, S.; Fygenson, D. Improving Fluorescence Detection in Lab on Chip Devices. *Lab Chip* **2008**, *8* (5), 649−652.

(12) Piorek, B. D.; Lee, S. J.; Santiago, J. G.; Moskovits, M.; Banerjee, S.; Meinhart, C. D. Free-Surface Microfluidic Control of Surface-Enhanced Raman Spectroscopy for the Optimized Detection of Airborne Molecules. *Proc. Natl. Acad. Sci. U. S. A.* **2007**, *104* (48), 18898−18901.

(13) Kahl, M.; Voges, E.; Kostrewa, S.; Viets, C.; Hill, W. Periodically Structured Metallic Substrates for SERS. *Sens. Actuators, B* **1998**, *51* (1), 285−291.

(14) Qian, X.; Zhou, X.; Nie, S. Surface-Enhanced Raman Nanoparticle Beacons Based on Bioconjugated Gold Nanocrystals and Long Range Plasmonic Coupling. *J. Am. Chem. Soc.* **2008**, *130* (45), 14934−14935.

(15) Tantra, R.; Brown, R. J. C.; Milton, M. J. T. Strategy to Improve the Reproducibility of Colloidal SERS. *J. Raman Spectrosc.* **2007**, *38* (11), 1469−1479.

(16) Ngo, Y. H.; Li, D.; Simon, G. P.; Garnier, G. Gold Nanoparticle−Paper as a Three-Dimensional Surface Enhanced Raman Scattering Substrate. *Langmuir* **2012**, *28* (23), 8782−8790.

(17) Santoro, G.; Yu, S.; Schwartzkopf, M.; Zhang, P.; Koyiloth Vayalil, S.; Risch, J. F. H.; Rubhausen, M. A.; Hernandez, M.; Domingo, C.; Roth, S. V. Silver Substrates for Surface Enhanced Raman Scattering: Correlation Between Nanostructure and Raman Scattering Enhancement. *Appl. Phys. Lett.* **2014**, *104* (24), 243107−243112.

(18) Wang, A. X.; Kong, X. Review of Recent Progress of Plasmonic Materials and Nano-Structures for Surface-Enhanced Raman Scattering. *Materials* **2015**, *8* (6), 3024−3052.

(19) Busà, C.; Rickard, J. J. S.; Chun, E.; Chong, Y.; Navaratnam, V.; Goldberg Oppenheimer, P. Tunable Superapolar Lotus-to-Rose hierarchical Nanosurfaces *via* Vertical Carbon Nanotubes Driven Electrohydrodynamic Lithography. *Nanoscale* **2017**, *9* (4), 1625−1636.

(20) Goldberg Oppenheimer, P.; Eder, D.; Steiner, U. Carbon Nanotube Alignment *via* Electrohydrodynamic Patterning of Nanocomposites. *Adv. Funct. Mater.* **2011**, *21* (10), 1895−1901.

(21) Goldberg Oppenheimer, P.; Hutter, T.; Chen, B.; Robertson, J.; Hofmann, S.; Mahajan, S. Optimized Vertical Carbon Nanotube Forests for Multiplex Surface-Enhanced Raman Scattering Detection. *J. Phys. Chem. Lett.* **2012**, *3* (23), 3486−3492.

(22) Goldberg Oppenheimer, P.; Steiner, U. Rapid Electrohydrodynamic Lithography Using Low-Viscosity Polymers. *Small* **2010**, *6* (11), 1248−1254.

(23) Rickard, J. J. S.; Farrer, I.; Goldberg Oppenheimer, P. Tunable Nanopatterning of Conductive Polymers *via* Electrohydrodynamic Lithography. *ACS Nano* **2016**, *10* (3), 3865−3870.

(24) Goldberg Oppenheimer, P.; Mahajan, S.; Steiner, U. Hierarchical Electrohydrodynamic Structures for Surface-Enhanced Raman Scattering. *Adv. Mater.* **2012**, *24* (23), OP175−OP180.

(25) Huang, J.-A.; Zhao, Y.-Q.; Zhang, X.-J.; He, L.-F.; Wong, T.-L.; Chui, Y.-S.; Zhang, W.-J.; Lee, S.-T. Ordered Ag/Si Nanowires Array: Wide-Range Surface-Enhanced Raman Spectroscopy for Reproducible Biomolecule Detection. *Nano Lett.* **2013**, *13* (11), 5039−5045.

(26) Liu, X.; Shao, Y.; Tang, Y.; Yao, K.-F. Highly Uniform and Reproducible Surface Enhanced Raman Scattering on Air-stable Metallic Glassy Nanowire Array. *Sci. Rep.* **2015**, *4* (1), 5835.

(27) Srichan, C.; Ekpanyapong, M.; Horprathum, M.; Eiamchai, P.; Nuntawong, N.; Phokharatkul, D.; Danvirutai, P.; Bohez, E.; Wisitsoraat, A.; Tuantranont, A. Highly-Sensitive Surface-Enhanced Raman Spectroscopy (SERS)-based Chemical Sensor Using 3D Graphene Foam Decorated with Silver Nanoparticles as SERS Substrate. *Sci. Rep.* **2016**, *6*, 23733.

(28) Schmidt, M. S.; Hübner, J.; Boisen, A. Large Area Fabrication of Leaning Silicon Nanopillars for Surface Enhanced Raman Spectroscopy. *Adv. Mater.* **2012**, *24* (10), OP11−OP18.

(29) Japan, S. http://www.stjapan.de/en/shop/accessories-for-spectroscopy-microanalysis/raman-sers-substrate/ (accessed 2020-05-29).
(30) StellarNet Inc. https://www.stellarnet.us/spectrometers-accessories/sers-substrates/ (accessed 2020-05-27).
(31) Analyzers, R.-T. http://sersitive.eu/shop/silver-substrate-5pcs-bundle/ (accessed 2020-05-29).
(32) Mesophotonics http://www.mesophotonics.com/products/klarite.html (accessed 2020-06-15).
(33) Jiao, Y.; Ryckman, J. D.; Ciesielski, P. N.; Escobar, C. A.; Jennings, G. K.; Weiss, S. M. Patterned Nanoporous Gold as an Effective SAB. *Nanotechnology* **2011**, *22* (29), 295302.
(34) Baltog, I.; Primeau, N.; Reinisch, R.; Coutaz, J. L. Surface Enhanced Raman Scattering on Silver Grating: Optimized Antenna-like Gain of the Stokes Signal of 10^4. *Appl. Phys. Lett.* **1995**, *66* (10), 1187−1189.
(35) Ward, D. R.; Grady, N. K.; Levin, C. S.; Halas, N. J.; Wu, Y.; Nordlander, P.; Natelson, D. Electromigrated Nanoscale Gaps for Surface-Enhanced Raman Spectroscopy. *Nano Lett.* **2007**, *7* (5), 1396−1400.
(36) Taminiau, T. H.; Stefani, F. D.; Segerink, F. B.; van Hulst, N. F. Optical Antennas Direct Single-molecule Emission. *Nat. Photonics* **2008**, *2* (4), 234−237.
(37) Xu, X.; Kim, K.; Li, H.; Fan, D. L. Ordered arrays of Raman nanosensors for Ultrasensitive and Location Predictable Biochemical Detection. *Adv. Mater.* **2012**, *24* (40), 5457−5463.
(38) Zhu, W.; Wen, B.-Y.; Jie, L.-J.; Tian, X.-D.; Yang, Z.-L.; Radjenovic, P. M.; Luo, S.-Y.; Tian, Z.-Q.; Li, J.-F. Rapid and Low-Cost Quantitative Detection of Creatinine in Human Urine with a Portable Raman Spectrometer. *Biosens. Bioelectron.* **2020**, *154*, 112067−112075.
(39) Cheng, H.-W.; Huan, S.-Y.; Wu, H.-L.; Shen, G.-L.; Yu, R.-Q. Surface-Enhanced Raman Spectroscopic Detection of a Bacteria Biomarker Using Gold Nanoparticle Immobilized Substrates. *Anal. Chem.* **2009**, *81* (24), 9902−9912.
(40) Szekeres, G. P.; Kneipp, J. SERS Probing of Proteins in Gold Nanoparticle Agglomerates. *Front. Chem.* **2019**, *7*, 30.
(41) Patel, T. B.; Clark, J. B. Synthesis of N-acetyl-L-aspartate by Rat Brain Mitochondria and its Involvement in Mitochondrial/cytosolic Carbon Transport. *Biochem. J.* **1979**, *184* (3), 539−546.
(42) Rickard, J. J. S.; Di-Pietro, V.; Smith, D. J.; Davies, D. J.; Belli, A.; Oppenheimer, P. G. Rapid Optofluidic Detection of Biomarkers for Traumatic Brain Injury *via* Surface-enhanced Raman Spectroscopy. *Nat. Biomed. Eng.* **2020**, *4*, 610.
(43) Shannon, R. J.; van der Heide, S.; Carter, E. L.; Jalloh, I.; Menon, D. K.; Hutchinson, P. J.; Carpenter, K. L. H. Extracellular N-Acetylaspartate in Human Traumatic Brain Injury. *Journal of neurotrauma* **2016**, *33* (4), 319−329.
(44) Socrates, G. *Infrared and Raman Characteristic Group Frequencies: Tables and Charts*, 3rd ed.; Wiley, 2004; pp 1−366.

https://dx.doi.org/10.1021/acsanm.0c01190
ACS Appl. Nano Mater. 2020, 3, 6774−6784